

1 Primary emissions versus secondary formation of fine particulate matter in the top polluted
2 city, Shijiazhuang, in North China

3 Ru-Jin Huang^{1,2}, Yichen Wang^{1,2}, Junji Cao^{1,2}, Chunshui Lin^{1,2,3}, Jing Duan^{1,2}, Qi Chen⁴, Yongjie Li⁵,
4 Yifang Gu^{1,2}, Jin Yan^{1,2}, Wei Xu^{1,2,3}, Roman Fröhlich⁶, Francesco Canonaco⁶, Carlo Bozzetti⁶, Jurgita
5 Ovadnevaite³, Darius Ceburnis³, Manjula R. Canagaratna⁷, John Jayne⁷, Douglas R. Worsnop⁷, Imad
6 El-Haddad⁶, André S. H. Prévôt⁶, Colin D. O'Dowd³

7 ¹Key Laboratory of Aerosol Chemistry and Physics, State Key Laboratory of Loess and Quaternary
8 Geology, Institute of Earth Environment, Chinese Academy of Sciences, Xi'an 710061, China

9 ²CAS Center for Excellence in Quaternary Science and Global Change, Xi'an, 710061, China

10 ³School of Physics and Centre for Climate and Air Pollution Studies, National University of Ireland
11 Galway, Galway, Ireland

12 ⁴State Key Joint Laboratory of Environmental Simulation and Pollution Control, College of
13 Environmental Sciences and Engineering, Peking University, Beijing, China

14 ⁵Department of Civil and Environmental Engineering, Faculty of Science and Technology, University
15 of Macau, Taipa, Macau, China

16 ⁶Laboratory of Atmospheric Chemistry, Paul Scherrer Institute (PSI), 5232 Villigen, Switzerland

17 ⁷Aerodyne Research, Inc., Billerica, MA, USA

18 *Correspondence to:* R.-J. Huang (rujin.huang@ieecas.cn)

19 **Abstract.** Particulate matter (PM) pollution is a severe environmental problem in the Beijing-Tianjin-
20 Hebei (BTH) region in North China. PM studies have been conducted extensively in Beijing, but the
21 chemical composition, sources, and atmospheric processes of PM are still relatively less known in the
22 nearby Tianjin and Hebei. In this study, fine PM in urban Shijiazhuang (the capital of Hebei province)
23 was characterized using an Aerodyne quadrupole aerosol chemical speciation monitor (Q-ACSM)
24 from 11 January to 18 February in 2014. The average mass concentration of non-refractory submicron
25 PM (diameter <1 μm , NR-PM₁) was $178 \pm 101 \mu\text{g m}^{-3}$ and composed of 50% organic aerosol (OA),

1 21% sulfate, 12% nitrate, 11% ammonium, and 6% chloride. Using the Multilinear Engine (ME-2)
2 receptor model, five OA sources were identified and quantified, including hydrocarbon-like OA from
3 vehicle emissions (HOA, 13%), cooking OA (COA, 16%), biomass burning OA (BBOA, 17%), coal
4 combustion OA (CCOA, 27%), and oxygenated OA (OOA, 27%). We found that secondary
5 formation contributed substantially to PM in episodic events, while primary emissions were dominant
6 (most significant) on average. The episodic events with the highest NR-PM₁ mass range of 300-360
7 $\mu\text{g m}^{-3}$ showed 55% of secondary species. On the contrary, a campaign-average low OOA fraction
8 (27%) in OA indicated the importance of primary emissions, and a low sulfur oxidation degree (F_{SO_4})
9 of 0.18 even at RH>90% hinted on insufficient oxidation. These results suggested that in wintertime
10 Shijiazhuang fine PM was mostly from primary emissions without sufficient atmospheric aging,
11 indicating opportunities for air quality improvement by mitigating direct emissions. In addition,
12 secondary inorganic and organic (OOA) species dominated in pollution events with high RH
13 conditions, most likely due to enhanced aqueous-phase chemistry, while primary organic aerosol
14 (POA) dominated in pollution events with low RH and stagnant conditions. These results also
15 highlighted the importance of meteorological conditions for PM pollution in this highly polluted city
16 in North China.

17 **1 Introduction**

18 Particulate pollution in China is a serious environmental problem, influencing air quality, regional and
19 global climate and human health. Especially during recent winters, large-scale and severe haze
20 pollution has brought China's particulate pollution at the forefront of world-wide media and evoking
21 great scientific interest in air pollution studies. Measurements at a number of major cities showed that
22 the wintertime daily average mass concentrations of PM_{2.5} (particulate matter with an aerodynamic
23 diameter <2.5 μm) are approximately 1-2 orders of magnitude higher than those observed in urban
24 areas in the US and European countries (Huang et al., 2014). Severe particulate pollution is often
25 accompanied by extremely poor visibility and poor air quality leading to a sharp increase in
26 respiratory diseases. Long-term exposure to high levels of particulate pollution is estimated to result
27 in 1.1 million deaths in 2015 in China, ranking the 1st in the world (Cohen et al., 2017).

1 The region of Beijing, Tianjin, and Hebei (BTH) is one of the important city clusters in China, but
2 also suffers from serious air pollution. Seven cities in this region ranked the top 10 most polluted
3 cities in China in the year 2014-2015 (<http://www.zhb.gov.cn>). The urgent need of an air quality
4 improvement in this region has been recognized by central and local governments as well as the
5 public, leading to mitigating actions being undertaken by the authorities. In particular, various
6 emission control measures were implemented in this region to clean Beijing's air, for example, during
7 the 2014 Asia-Pacific Economic Cooperation (APEC) summit. These temporal measures include the
8 odd-even ban on vehicles and shutdowns of factories and construction sites, leading to serious side
9 effects on daily life and economic growth. Therefore, identification of the major sources and
10 atmospheric processes producing airborne particles is required for implementing targeted and
11 optimized emission control strategies.

12 The first step for quantifying the PM sources requires the measurements of inorganic and organic
13 tracers and/or mass spectrometric fingerprints of ambient PM samples. This can be realized by the
14 online ambient measurements using aerosol mass spectrometric (AMS) techniques to determine
15 aerosol composition (Jimenez et al., 2009; Ng et al., 2011b; Elser et al., 2016b). In particular, the
16 quadrupole aerosol chemical speciation monitor (Q-ACSM) and recently time-of-flight aerosol
17 chemical speciation monitor (TOF-ACSM) have been developed for long-term continuous
18 measurements of the non-refractory submicron aerosols (Ng et al., 2011a; Fröhlich et al., 2013).
19 Aerosol sources have been successfully identified from the AMS measurements with positive matrix
20 factorization (PMF) analysis (Ulbrich et al., 2009; Crippa et al., 2013; Elser et al., 2016a). In terms of
21 Q-ACSM datasets, the use of PMF often fails to resolve sources with similar mass spectral profiles,
22 e.g. the mixing of cooking organic aerosol with traffic organic aerosol in Nanjing (Zhang et al.,
23 2015b); or those present in low contributions, e.g. the lack of success in resolving a factor related to
24 biomass burning in Beijing (Jiang et al., 2015). It was also pointed out that PMF cannot separate the
25 aerosol sources of temporal covariations driven by low temperature and periods of strong inversions
26 (Canonaco et al., 2013; Reyes et al., 2016). Several source apportionment studies (in which PMF did
27 not find optimal results) have utilized the multilinear engine (ME-2) solver, which enables constraint
28 of the factor profiles/time series, providing a superior separation of the PM sources (e.g., Canonaco et

1 al., 2013; Canonaco et al., 2015; Fröhlich et al., 2015a; Fröhlich et al., 2015b; Minguillón et al., 2015;
2 Petit et al., 2015; Ripoll et al., 2015; Reyes et al., 2016; Bressi et al., 2016; Schlag et al., 2016; Wang
3 et al., 2017; Zhu et al., 2018). However, studies using ME-2 to resolve OA sources from the ACSM
4 measurements are scarce in the BTH region.

5 Apart from the lack of applications of ME-2 for the OA source apportionment, most of the field
6 studies have mainly focused on the aerosol pollution in Beijing (Sun et al., 2013; Sun et al., 2014; Sun
7 et al., 2016; Jiang et al., 2015; Xu et al., 2015; Elser et al., 2016b; Hu et al., 2016a). These and related
8 studies have clearly shown that Beijing is sensitive to the regional transport of aerosols from its
9 surrounding areas (Xu et al., 2008; Zhang et al., 2012; Li et al., 2015a). For example, Guo et al.
10 (2010) estimated that the regional pollutants on average accounted for 69% of PM_{10} and 87% of $PM_{1.8}$
11 in Beijing during summer, with sulfate, ammonium, and oxalate mostly formed regionally (regional
12 contributions >87%). Sun et al. (2014) reported that 66% of NR- PM_1 was from regional transport in
13 Beijing during the 2013 winter haze event. Among the surrounding areas of Beijing, the Hebei
14 province is the main source area leading to high aerosol loadings in Beijing (Chen et al., 2007; Xu et
15 al., 2008; Lang et al., 2013; Li et al., 2015a).

16 Shijiazhuang, the capital of Hebei province, is located ~270 km south of Beijing and has a population
17 approximately half that of Beijing. Zhao et al. (2013a, b) characterized the spatial and seasonal
18 variations of $PM_{2.5}$ chemical composition in the BTH region, and Shijiazhuang was selected as the
19 representative of the polluted cities in Hebei province. The off-line analysis results showed that
20 organic carbon (OC) and elemental carbon (EC) concentrations in Shijiazhuang were lower in the
21 spring and summer than those in the autumn and winter. The sum of secondary inorganic species
22 (SO_4^{2-} , NO_3^- , and NH_4^+) was highest in the autumn. Yet the temporal profiles of PM composition
23 cannot be captured by off-line analyses, hindering more detailed study on the sources and formation
24 of PM. In this work, we present for the first time the 30-minute time resolved NR- PM_1 measurements
25 in Shijiazhuang during the winter heating season. The characteristics of NR- PM_1 are analyzed, which
26 include (1) time series, mass fraction and diurnal variation of NR- PM_1 species; (2) multilinear engine
27 (ME-2)-resolved OA sources and their mass fraction as well as their diurnal variation; and (3) the

1 characteristics and atmospheric evolution of aerosol composition and sources under different aerosol
2 loadings and meteorological conditions.

3 **2 Methods**

4 **2.1 Sampling site**

5 Shijiazhuang, the capital of Hebei province, is located ~270 km south of Beijing. In 2014, ~10 million
6 residents and 2.1 million vehicles were reported in this city. It is often ranked the first in the list of top
7 10 most polluted cities in China, especially during wintertime heating periods (from 15 November to
8 15 March of the next year). For example, the average concentration of PM_{2.5} was 226.5 µg m⁻³ with
9 the peak hourly concentration of 933 µg m⁻³ during the 2013-2014 wintertime heating period, largely
10 exceeding the Chinese air pollution limit of 75 µg m⁻³. In this study, we performed an intensive field
11 measurement campaign at an urban site in Shijiazhuang to investigate the chemical composition,
12 sources and atmospheric processes of fine particles. The campaign was carried out from 11 January to
13 18 February 2014 on the building roof (15 m) of the Institute of Genetics and Developmental Biology,
14 Chinese Academy of Sciences (38°2'3''N, 114°32'29''E), a site located in a residential-business
15 mixed zone.

16 **2.2 Instrumentation**

17 NR-PM₁ was measured with an Aerodyne quadrupole aerosol chemical speciation monitor (Q-
18 ACSM), which can provide quantitative mass concentration and mass spectra of non-refractory
19 species including organics, sulfate, nitrate, ammonium, and chloride. The operation principles of Q-
20 ACSM can be found elsewhere (Ng et al., 2011a). The ambient aerosol was drawn through a Nafion
21 dryer (Perma Pure PD-50T-24SS) following a URG cyclone (Model: URG-2000-30ED) with a cut-off
22 size of 2.5 µm to remove coarse particles. The sampling flow was ~3 L min⁻¹, of which ~85 mL min⁻¹
23 was isokinetically sampled into the Q-ACSM. The residence time in the sampling tube was ~5 s. The
24 Q-ACSM was operated with a time resolution of 30 min and scanned from *m/z* 10 to 150 at 200 ms
25 amu⁻¹. Dry mono-dispersed 300-nm ammonium nitrate and ammonium sulfate particles (selected by a
26 differential mobility analyzer, DMA, TSI model 3080) were nebulized from a custom-built atomizer
27 and sampled into the Q-ACSM and a condensation particle counter (CPC, TSI model 3772)

1 calibrating ionization efficiency (IE). IE can, therefore, be determined by comparing the response
2 factors of Q-ACSM to the mass calculated with the known particle size and the number concentration
3 from CPC.

4 Ozone (O₃) was measured by a Thermo Scientific Model 49i ozone analyzer, CO by a Thermo
5 Scientific Model 48i carbon monoxide analyzer, SO₂ by an Ecotech EC 9850 sulfur dioxide analyzer,
6 and NO₂ by a Thermo Scientific Model 42i NO-NO₂-NO_x analyzer. The meteorological data,
7 including temperature, relative humidity (RH), precipitation, wind speed and wind direction, were
8 measured by an automatic weather station (MAWS201, Vaisala, Vantaa, Finland) and a wind sensor
9 (Vaisala Model QMW101-M2).

10 **2.3 Data analysis**

11 **2.3.1 Q-ACSM data analysis**

12 The mass concentrations and composition of NR-PM₁ were analyzed with the standard Q-ACSM data
13 analysis software written in Igor Pro (WaveMetrics, Inc., OR, USA). Standard relative ionization
14 efficiencies (RIEs) were used for organics, nitrate and chloride (i.e., 1.4 for organics, 1.1 for nitrate
15 and 1.3 for chloride) (Ng et al., 2011a) and RIEs for ammonium (6.0) and sulfate (1.2) were derived
16 from the IE calibrations. The particle collection efficiency (CE) was applied to correct for the particle
17 loss at the vaporizer due to particle bounce, which is influenced by aerosol acidity, composition, and
18 the aerosol water content. Given that aerosol was dried before entering into Q-ACSM and that
19 ammonium nitrate mass fraction (ANMF) during the observation period was lower than 0.4, the
20 composition dependent CE was estimated following the method described in Middlebrook et al.
21 (2012).

22 **2.3.2 The Multilinear Engine (ME-2)**

23 PMF is a bilinear receptor model that represents an input data matrix as a linear combination of a set
24 of factor profiles and their time-dependent concentrations (Paatero and Tapper, 1994). Factors
25 typically correspond to unique sources and/or processes. This allows for a quantitative apportionment
26 of bulk mass spectral time series into several factors through the minimization of a quantity Q , which

1 is the sum of the squares of the error-weighted residuals of the model. The PMF-AMS/ACSM
2 analyses have been widely used for apportioning the sources of organic aerosol. However, in
3 conventional PMF analyses, rotational ambiguity with limited rotational controls can lead to unclear
4 factor resolution, especially in China where the emission sources are very complex and covariant
5 during haze events. In contrast, the multi-linear engine (ME-2), used in this study, enables efficient
6 exploration of the entire solution space and can direct the apportionment towards an environmentally-
7 meaningful solution through the constraints of a subset of priori factor profiles or time series using the
8 *a* value approach (Canonaco et al., 2013). The *a* value can vary between 0 and 1. An *a* value of 0.1
9 accounts for maximum $\pm 10\%$ variability of each *m/z* signal of the final solution spectra that may
10 differ from the anchor, implying that some *m/z* signals might increase while some might decrease.

11 The source finder (SoFi, Canonaco et al., 2013) tool version 4.9 for Igor Pro was used for ME-2 input
12 preparation and result analysis. The number of factors resolved is determined by the user and the
13 solutions of the model are not mathematically unique due to rotational ambiguity. It is, therefore,
14 critical to study other parameters, e.g., the chemical fingerprint of the factor profiles, diurnal cycles,
15 and time series of factors and external measurements, to support factor identification and
16 interpretation (Canonaco et al., 2013; Crippa et al., 2014, Elser et al., 2016b).

17 **3 Results and discussion**

18 **3.1 Concentration and chemical composition of NR-PM₁**

19 Fig. 1 shows the time series of NR-PM₁ species, trace gases and meteorological conditions during the
20 entire measurement period. The measured mass concentrations of NR-PM₁ for the entire campaign
21 period ranged from a few $\mu\text{g m}^{-3}$ to $508.4 \mu\text{g m}^{-3}$, with an average of $178 \pm 101 \mu\text{g m}^{-3}$. That was
22 much higher than the wintertime/summertime concentrations measured in many other cities (see
23 Table 1). The mass concentration of NR-PM₁ correlated strongly with that of PM_{2.5} ($R^2 = 0.76$) with a
24 regression slope of 0.72, indicating that NR-PM₁ represents a majority of PM_{2.5} mass. The NR-PM₁
25 concentrations exceeded the Chinese PM_{2.5} limit of $75 \mu\text{g m}^{-3}$ for 90% of days during the
26 measurement period, showing the severity of particulate air pollution at Shijiazhuang.

1 Similar to measurements at other urban sites, OA was the dominant fraction of NR-PM₁, with an
2 average of 50% (31-80%), followed by 21% of sulfate (4-36%), 12% of nitrate (2-26%), 11% of
3 ammonium (4-21%) and 6% of chloride (2-20%). The dominant contribution of organics in NR-PM₁
4 is also consistent with measurements from other urban sites in the BTH region during winter heating
5 seasons (see Table 1). Sulfate was the second largest contributor to NR-PM₁. The large fraction of
6 sulfate was likely associated with the large consumption of coal in Hebei province, i.e., 296 million
7 tons in 2014 were used in coal-fired power plants and steel industry (producing ~11% of global steel
8 output in 2014). The enhancement of chloride fraction from >1-4% in other Chinese cities in summer
9 (see Table 1) to 6% in Shijiazhuang in winter (within the range of >2-7% in other Chinese cities in
10 winter, see Table 1) can be attributed to the substantial emissions from coal and/or biomass burning
11 activities.

12 Fig. 2a shows the diurnal variations of NR-PM₁ components, which were affected by the evolution of
13 the planetary boundary layer (PBL) height that governed the vertical dispersion of pollutants and by
14 the diurnal cycle of the emissions and atmospheric processes. The concentrations of pollutants
15 increased at night as a result of enhanced emissions from residential heating (in particular, for
16 organics and chloride) and a progressively shallower PBL. During daytime the PBL height was
17 developed by solar radiation and thus the pollutants became diluted resulting in the decrease of
18 organics, sulfate, ammonium and chloride in the afternoon. In contrast, the concentrations of nitrate
19 increased after sunrise but then kept rather constant throughout the afternoon, suggesting a strong
20 source or production of nitrate which offsets the dilution from PBL development. To minimize the
21 effects from PBL heights, data were normalized by ΔCO . CO is often used as an emission tracer to
22 account for dilution on timescales of hours to days because of its relatively long life time against the
23 oxidation by OH radicals (approximately one month) (Decarlo et al., 2010). After offsetting the PBL
24 dilution effect, sulfate, nitrate and ammonium showed clear increases from 7:00 to 15:00 (Fig. 2c),
25 indicating efficient daytime production of these secondary inorganic species. It should be noted that
26 the increase of nitrate (about 2 times, from $\sim 6 \mu\text{g m}^{-3} \text{ppm}^{-1}$ to $\sim 12 \mu\text{g m}^{-3} \text{ppm}^{-1}$) is slightly larger
27 than that of sulfate (about 1.6 times, from $\sim 11 \mu\text{g m}^{-3} \text{ppm}^{-1}$ to $\sim 17.5 \mu\text{g m}^{-3} \text{ppm}^{-1}$), indicating more
28 efficient photochemical production of nitrate than sulfate, given that the loss rate of sulfate could not

1 be higher than that of nitrate as nitric acid is semi-volatile and may be further lost by evaporation.
2 Also, the continuous increase of organics after sunrise suggested efficient photochemical production
3 of secondary organic aerosol (SOA).

4 **3.2 Sources of organic aerosol**

5 From the PMF analysis, we first examined a range of solutions with 3 to 8 factors. The solution that
6 best represents the data is the 5-factor solution (Fig. S1). The solutions with factor numbers more than
7 5 provide no new meaningful factors (see Fig. S2 and more details in the supplementary material).

8 Although the 5-factor solution can reasonably represent the data, HOA is still mixed with BBOA
9 because the HOA profile contains higher than expected contribution from m/z 60. In addition, COA
10 contains no signal at m/z 44, which might indicate a suboptimal splitting between the contributing
11 sources. To better separate HOA from BBOA, we constrained the HOA profile from Ng et al (2011b),
12 which is an average profile over 15 cities from China, Japan, Europe and the United States. Although
13 gasoline vehicles dominate in China while diesel vehicles dominate in Europe, HOA mass spectra do
14 not show significant variability when compared to different sites in China and Europe (Ng et al.,
15 2011b; Reyes et al., 2016; Bozzetti et al., 2017), indicating that traffic emissions from different types
16 of vehicles have similar profiles. To avoid the influences of other sources on COA, the COA profile
17 from Paris (Crippa et al., 2013) was used as a constraint because high similarities were found between
18 the COA profile from Paris and four COA profiles from different types of Chinese cooking activities
19 (He et al., 2010; Crippa et al., 2013). However, the constraint on HOA and COA profiles still seems
20 to sub-optimally resolve the apportionment of BBOA from CCOA, as one unconstrained factor
21 contains high contributions from both m/z 60 and PAH-related m/z 's (m/z 77, 91 and 115, as shown in
22 Fig. S3) which indicate the mixing between BBOA and CCOA. To separate BBOA and CCOA, we
23 constrained BBOA using the average of BBOA profiles from the 5-factor unconstrained PMF
24 solutions.

25 To explore the solution space, a value of 0-0.5 with an interval of 0.1 was used to constrain both the
26 HOA and COA reference profiles from literature while BBOA was constrained with a value of 0
27 because the BBOA profile was resolved from unconstrained PMF solution which is not expected to

1 vary significantly. 36 possible results were obtained by limiting a range of a values. Three criteria for
2 optimizing OA source appointment are as follows:

3 (1) *The diurnal pattern of COA*. The diurnal cycle of COA should have higher concentrations
4 during mealtime.

5 (2) *Minimization of m/z 60 in HOA*. The upper limit of m/z 60 in the HOA profile is 0.006, which
6 is the maximal fractional contribution derived from multiple ambient data sets in different
7 regions (mean + 2σ) (Ng et al., 2011b).

8 (3) *The rationality of unconstrained factors*. OOA should have abundant signal at m/z 44 and
9 contain much lower signals at PAH-related ion peaks compared to CCOA.

10 Nine solutions match the criteria above. The final time series and mass spectra are therefore the
11 averages of these 9 solutions. The diurnal variations of mass concentrations of the OA factors and
12 their PBL-corrected results are shown in Fig. 2b and d, respectively. The mass spectra and time series
13 of the OA factors and their correlation with external tracers are shown in Fig. 3. The relative
14 contributions of each OA source to the m/z 's are shown in Fig. S4. Potential source contribution
15 function (PSCF) analysis was also performed and the result is shown in Fig. S5.

16 OOA is characterized by high signals at m/z 44 (CO_2^+) and m/z 43 (C_3H_7^+ or $\text{C}_2\text{H}_3\text{O}^+$). OOA accounts
17 for 85% of m/z 44 signal, much higher than other OA sources. The time series of OOA is highly
18 correlated with that of sulfate ($R^2=0.70$), nitrate ($R^2=0.75$) and ammonium ($R^2=0.76$), confirming the
19 secondary nature of this factor. The diurnal cycle of OOA shows an increase from 7:00 to 11:00,
20 followed by a decrease in the afternoon due to the PBL evolution effect. After normalizing the PBL
21 effect, OOA increased continuously from 7:00 to 15:00, indicating the importance of photochemical
22 oxidation. This diurnal feature together with the PSCF results indicated that a large fraction of OOA
23 was produced locally and/or produced from the highly populated and industrialized surrounding areas,
24 consistent with the sulfate production discussed below.

25 The mass spectrum of CCOA is featured by prominent contributions of unsaturated hydrocarbons,
26 particularly PAH-related ion peaks (e.g., 77, 91, and 115). The CCOA profile shows a weaker signal

1 at m/z 44 than that observed in Beijing (Hu et al., 2016a) and Lanzhou (Xu et al., 2016). This
2 difference can be caused by the difference in coal types, burning conditions and aging processes
3 (Zhou et al., 2016). CCOA accounts for 42-66% of PAH-related ion peaks, much higher than those in
4 other OA sources. This result suggested that the major source of PAHs was coal combustion in
5 wintertime Shijiazhuang. The campaign-averaged mass concentration of CCOA was $23.2 \mu\text{g m}^{-3}$,
6 which is higher than that in Xi'an ($10.1 \mu\text{g m}^{-3}$) but is similar to that in Beijing ($23.5 \mu\text{g m}^{-3}$) observed
7 in the same winter (Elser et al., 2016a). Nevertheless, during haze extremes, the average CCOA
8 concentration was $77.5 \mu\text{g m}^{-3}$ in Shijiazhuang, much higher than that in Beijing ($48.2 \mu\text{g m}^{-3}$, Elser et
9 al., 2016a). CCOA showed distinct diurnal variations with low concentration down to $12.6 \mu\text{g m}^{-3}$
10 during the day and high concentration up to $37.6 \mu\text{g m}^{-3}$ at night, corresponding to 19% and 35% of
11 OA, respectively. The elevated CCOA concentrations at night suggested a large emission from
12 residential heating activities using coal as the fuel compounded by the shallow PBL. The average
13 contribution of CCOA to the total OA was 27%, which is consistent with studies in Beijing and
14 Handan (~160 km south to Shijiazhuang) where CCOA was found to be the dominant primary OA
15 (Elser et al., 2016a; Sun et al., 2016; Li et al., 2017). Given this large fraction of OA from coal
16 combustion, mitigating residential coal combustion is therefore of significant importance for
17 improving air quality in the BTH regions.

18 The BBOA mass spectrum is featured by prominent m/z 60 (mainly $\text{C}_2\text{H}_4\text{O}_2^+$) and 73 (mainly
19 $\text{C}_3\text{H}_5\text{O}_2^+$) signals (He et al., 2010). These two ions ($\text{C}_2\text{H}_4\text{O}_2^+$ and $\text{C}_3\text{H}_5\text{O}_2^+$) are fragments of
20 anhydrous sugars produced from the incomplete combustion and pyrolysis of cellulose and
21 hemicelluloses (Alfarra et al., 2007; Lanz et al., 2007; Mohr et al., 2009). Consistently, BBOA
22 accounts for 50% of m/z 60 and 56% of m/z 73, much higher than those in other sources. In addition,
23 BBOA accounts for 9-27% of the PAH-related m/z 's (i.e., m/z 77, 91 and 115), lower than that in
24 CCOA but higher than those in other primary OA sources. This suggested that BBOA was also an
25 important PAH source in wintertime Shijiazhuang. A high correlation was found between the time
26 series of BBOA and that of chloride ($R^2=0.75$), the latter of which was suggested to be one of the
27 tracers of biomass burning. BBOA on average accounted for 17% of OA, which is higher than those
28 (9-12%) observed in Beijing during wintertime heating seasons (Elser et al., 2016a; Hu et al., 2016a;

1 Sun et al., 2016). The higher BBOA contribution in wintertime Shijiazhuang is likely associated with
2 widespread use of wood and crop residuals for heating and cooking in Shijiazhuang and surrounding
3 areas, as supported by the PSCF results (Fig. S5).

4 The COA profile is characterized by a high m/z 55/57 ratio of 2.7, much higher than that in non-
5 cooking POA (0.6-1.1) but within the range of 2.2-2.8 in COA profiles reported by Mohr et al.
6 (2012). COA shows a clear diurnal cycle with distinct peaks at lunch (between 11:00-13:00 local
7 time, LT) and dinner (between 19:00-21:00 LT) times. A small peak was also observed in the
8 morning between 06:00 and 07:00 LT, consistent with the breakfast time. COA on average accounted
9 for 16% of total OA with the highest contribution of 24% during dinner time.

10 The HOA mass spectrum is dominated by hydrocarbon ion series of $[C_nH_{2n+1}]^+$ and $[C_nH_{2n-1}]^+$
11 (Canagaratna et al., 2004; Mohr et al., 2009). The diurnal variation of HOA is featured by high
12 concentration at night, likely due to enhanced truck emissions (only allowed to drive on road from
13 23:00 to 6:00 LT) and shallow PBL at night. Similar diurnal cycles were found in wintertime Beijing
14 and Xi'an (Sun et al., 2016; Elser et al., 2016a). HOA, on average, accounted for 13% of total OA for
15 the entire observation period, which was higher than that in Beijing (9-10%) but lower than that in
16 Xi'an (15%) measured in the same winter (Elser et al., 2016a; Sun et al., 2016).

17 **3.3 Chemical nature and sources at different PM levels**

18 Fig. 4 shows the mass fractions of NR-PM₁ species and OA sources on reference days and extremely
19 polluted days. Here, the days with NR-PM₁ daily average mass concentration higher than the 75th
20 percentile (i.e., $\geq 238 \mu\text{g m}^{-3}$) are denoted as the extremely polluted days and the rest of days as
21 reference days. The average concentration of NR-PM₁ was $310 \mu\text{g m}^{-3}$ during extremely polluted
22 days, about 2 times higher than that during reference days ($162 \mu\text{g m}^{-3}$). The average concentration of
23 secondary inorganic aerosol was $65 \mu\text{g m}^{-3}$ (40% of NR-PM₁ mass) during reference days and
24 increased to $143 \mu\text{g m}^{-3}$ (46% of NR-PM₁ mass) during extremely polluted days. Secondary organic
25 aerosol also increased from $19 \mu\text{g m}^{-3}$ (22% of OA) during reference days to $40 \mu\text{g m}^{-3}$ (26% of OA)
26 during extremely polluted days. The enhanced mass concentrations (~ 2 times) of both secondary
27 inorganic aerosol and secondary organic aerosol during extremely pollution days suggested strong

1 secondary aerosol production during pollution events. Such enhancement was likely confounded by
2 stagnant weather conditions (e.g., average wind speed was 0.9 m s^{-1}) and high RH of 69.4% which
3 facilitated the production and accumulation of secondary aerosol. Note that it was already very
4 polluted during the reference days with an average concentration of NR-PM₁ of $162 \mu\text{g m}^{-3}$, which
5 may explain the relatively small increase in fractional contribution of secondary aerosol from
6 reference days to extremely polluted days.

7 Fig. 5a and b show the factors driving the pollution events by binning the fractional contribution of
8 each chemical species and OA source to total NR-PM₁ and OA mass, respectively. The data clearly
9 show that high pollution events are characterized by an increasing secondary fraction, reaching ~55%
10 at the highest NR-PM₁ mass bin ($300\text{-}360 \mu\text{g m}^{-3}$). In particular, from the lowest NR-PM₁ bin to the
11 highest NR-PM₁ bin, the fractional contribution increases from 14% to 25% for sulfate in NR-PM₁
12 and from 18% to 25% for OOA in OA, demonstrating the importance of secondary aerosol formation
13 in driving particulate air pollution (Huang et al., 2014; Elser et al., 2016; Wang et al., 2017). To
14 investigate the oxidation degree of sulfur at different NR-PM₁ mass, the sulfur oxidation ratio (F_{SO_4})
15 was calculated according to Eq. (1)

$$F_{\text{SO}_4^{2-}} = \frac{n[\text{SO}_4^{2-}]}{n[\text{SO}_4^{2-}] + n[\text{SO}_2]} \quad (1)$$

16
17 where n is the molar concentration. As can be seen from Fig. 6, F_{SO_4} shows a clear increase trend with
18 NR-PM₁ mass, increasing from 0.08 in the lowest mass bin to 0.21 in the highest mass bin. However,
19 the highest F_{SO_4} value is still much lower than that reported in previous studies, e.g., 0.62 in Xi'an
20 (Elser et al., 2016), suggesting low atmospheric oxidative capacity during the measurement period in
21 Shijiazhuang. This may also explain the relatively low OOA fraction (see Fig. 5b). Certainly, it
22 should be noted that the mass concentration of sulfate may also be affected by other parameters
23 including aerosol liquid water content, aerosol or cloud water pH, besides atmospheric oxidative
24 capacity.

3.4 Evolution of aerosol composition and sources at different RH levels

Fig. 7a and b show the mass concentrations of the NR-PM₁ species and of the OA sources as a function of RH, with RH bins of 10% increments. The absolute mass concentrations of secondary inorganic species increased as RH increased from 60%, while chloride showed a decreasing trend. Among the OA sources, OOA and HOA were enhanced with RH increasing from <60% to 90%, while other OA sources did not show a clear trend. As RH increased gradually with the decrease of wind speed (Fig. 6a), the development of stagnant weather conditions (including a shallower PBL) promoted both the accumulation of pollutants and the formation of secondary aerosol (Tie et al., 2016). To minimize the effects from PBL variations, the NR-PM₁ species and OA fractions were normalized by the sum of the POA, as a surrogate of secondary aerosol precursors. The resulting ratios were further normalized by the values at the first RH bin (<60%) for better visualization. As shown in Fig. 7c, when RH increased from 60% to 100%, the normalized sulfate increased by a factor of ~1.7, suggesting the importance of aqueous-phase SO₂ oxidation in the formation of sulfate at high RH. The enhancements for nitrate and ammonium were slightly lower (~1.2) compared to that sulfate, because NH₄NO₃ is thermally labile and its gas-particle partitioning is affected by both temperature and RH. The importance of aqueous-phase chemistry is further supported by the increase of F_{SO_4} as a function of RH (Fig. 6b). At RH <60%, F_{SO_4} was rather constant, with an average of 0.09, indicating a low sulfur oxidation degree. At RH >60%, F_{SO_4} increased rapidly with the increase of RH, reaching a maximal average of 0.18 at the last RH bin (90-100%). Note that the sulfur oxidation degree at high RH (>60%) was much lower compared to those measured in Xi'an during the same winter (average F_{SO_4} 0.62 at RH=90-100%, Elser et al., 2016a). The low sulfur oxidation degree observed in Shijiazhuang (i.e., >80% of sulfur is still not oxidized) indicated insufficient atmospheric processing and also suggested a large fraction of pollutants in Shijiazhuang was likely emitted locally and/or transported from the heavily populated and industrialized surrounding areas. With a longer atmospheric processing time in the downwind region, e.g., Beijing, higher secondary aerosol fractions are expected, as observed in previous studies (e.g., Huang et al., 2014). Similar to sulfate, the normalized OOA increased by a factor of ~1.2 when RH increased from 60% to 100% (Fig. 7d). The mass fraction of OOA increased from 29% to 41% when RH increased from 70% to 100%, while

1 POA contribution decreased correspondingly from 71% to 59% (Fig. 6d). These results support the
2 above discussion that aqueous-phase chemistry also plays an important role in the formation of OOA
3 under high RH conditions during haze pollution episodes.

4 **3.5 Primary emissions versus secondary formation**

5 Frequent changes between clean and polluted episodes were observed in this study. To get a better
6 insight into aerosol sources and atmospheric processes, 4 clean periods (C1-C4) with daily average
7 mass concentration of NR-PM₁ lower than the 25th percentile, 6 high-RH (>80%) polluted episodes
8 (H1-H6) and 4 low-RH (<60%) polluted episodes (L1-L4) with daily average mass concentration of
9 NR-PM₁ higher than the 75th percentile were selected for further analysis. As shown in the Fig. 8, the
10 chemical composition and sources differed during different episodes. The contributions of organics
11 showed a decreasing trend, from 54-64% during C1-C4 to 49-58% during L1-L4, and to 35-44%
12 during H1-H6, while the corresponding contributions of secondary inorganic species increased. This
13 indicated a notable production and accumulation of secondary inorganic aerosol during severe haze
14 pollution events. For example, the mass fraction of sulfate in NR-PM₁ was much higher during high
15 RH pollution events (H1-H6, 27-30%) compared to those during low RH pollution events (L1-L4, 11-
16 18%) and clean events (C1-C4, 11-17%). OOA also showed a much higher contribution to OA during
17 high RH pollution events (H1-H6, 29-50%) than during low RH pollution events (L1-L3, 17-26%)
18 and clean events (C1-C4, 10-34%). Interestingly, when comparing high RH and low RH pollution
19 events of similar PM levels (Fig. 8), secondary inorganic species and OOA dominated the particulate
20 pollution at high RH pollution events likely due to enhanced secondary formation, similar to previous
21 studies (e.g., Wang et al., 2017), while POA dominated the particulate pollution at low RH and under
22 stagnant conditions. The concentrations of POA are determined by both emissions and meteorological
23 conditions. The different significance of primary aerosol and secondary aerosol in low and high RH
24 pollution events highlights the importance of meteorological conditions in driving particulate
25 pollution.

26 Fig. 9 shows the evolution of aerosol species in two cases of different RH levels. The first case had
27 average RH <50% from 20-24 Jan (C2 and L3 episodes). The high wind speed (>6 m s⁻¹) from the

1 northwest before the L3 episode led to a significant reduction of air pollutants (the C3 episode, a
2 clean-up period). When the wind direction switched from northwest to 90°-270° sector and the wind
3 speed decreased to $<3 \text{ m s}^{-1}$, the measured pollutants (except O_3 which was reacted out by increasing
4 NO emissions) started to build up. Specifically, NR-PM_{10} showed a dramatic increase by a factor of 19
5 over the first 11 hours (from 20 Jan 16:00 to 21 Jan 3:00 LT) from 12 to $233 \mu\text{g m}^{-3}$. In this process
6 POA contributed to an average 69% of NR-PM_{10} mass. The other three processes were also
7 characterized by a rapid increase of NR-PM_{10} mass ($39\text{-}50 \mu\text{g m}^{-3} \text{ h}^{-1}$) and high contribution of POA,
8 i.e., from 22 Jan 0:00-22 Jan 3:00, 22 Jan 16:00-22 Jan 20:00, and 23 Jan 12:00-23 Jan 19:00. Such
9 rapid increases in NR-PM_{10} mass under low RH were associated with stagnant weather conditions
10 (e.g., low wind speed) which promoted the accumulation of pollutants. The second case had average
11 $\text{RH} > 80\%$ from 5-8 Feb (H3 and H4 episodes). In this case, the wind speed was low ($<3 \text{ m s}^{-1}$)
12 throughout the 4-day period. Under this very stagnant weather condition, POA accumulated
13 continuously (Fig. 9). However, different from the low-RH case, the concentration of secondary
14 species also showed continuous increases in this high-RH case. The enhancement of secondary
15 aerosol formation was likely driven by aqueous-phase chemistry at high RH level (Elser et al., 2016;
16 Wang et al., 2017) and the accumulation of pollutants under stagnant weather conditions (Tie et al.,
17 2017) which further promoted the formation of secondary species.

18 **4 Conclusions**

19 The chemical nature, sources and atmospheric processes of wintertime fine particles in Shijiazhuang
20 were investigated. The mass fractions of secondary inorganic species and SOA increased with the
21 increase of NR-PM_{10} mass, suggesting the importance of secondary formation in driving PM pollution.
22 However, the low sulfur oxidation degree and low OOA fraction indicated insufficient atmospheric
23 oxidation capacity. Together with the diurnal variations and PSCF results, these observations
24 suggested that a large fraction of pollutants in Shijiazhuang was most likely produced locally and/or
25 transported from the heavily populated and industrialized surrounding areas without sufficient
26 atmospheric aging. Two different regimes were found to be responsible for the high PM pollution in
27 Shijiazhuang. At low RH under stagnant weather conditions, the accumulation of primary emissions

1 was the main culprit. In contrast, at high RH, the enhanced formation of secondary aerosol through
2 aqueous-phase chemistry was the main culprit. To conclude, we found that in this highly polluted city
3 in North China, (1) secondary formation is important in high-PM episodes, (2) primary emissions are
4 still important on an average basis, and (3) meteorological conditions play an important part in
5 pollutant accumulation and transformation. The findings from this study thus suggest that (a) there are
6 still opportunities for air pollution mitigation by controlling direct emissions such as coal combustion,
7 and (b) control on precursors (e.g., NO_x, SO₂, and VOCs) for secondary formation, especially during
8 high-PM episodes with unfavorable meteorological conditions, can ease the situation substantially.

9 **Author Contribution**

10 RJH and JC designed the study. YW and RJH performed the measurements. RJH, YW, CL, JD, QC
11 and YL analyzed and interpreted the data. RJH, YW and JD wrote the manuscript with contribution
12 from all co-authors.

13 **Competing interests**

14 The authors declare that they have no conflict of interest.

15 **Acknowledgement**

16 This research is supported by the National Science Foundation of China (No. 91644219, 41877408,
17 and 41675120), the National Key Research and Development Program of China (no.
18 2017YFC0212701), and EPA-Ireland (AEROSOURCE, 2016-CCRP-MS-31).

20 **References**

- 21 Alfarra, M. R., Prévôt, A. S. H., Szidat, S., Sandradewi, J., Weimer, S., Schreiber, D., Mohr, M., and
22 Baltensperger, U.: Identification of the mass spectral signature of organic aerosols from wood burning
23 emissions, *Environ. Sci. Technol.*, 41, 5770–5777, 2007.
- 24 Bozzetti, C., El Haddad, I., Salameh, D., Daellenbach, K. R., Fermo, P., Gonzalez, R., Minguillón, M.
25 C., Iinuma, Y., Poulain, L., Müller, E., Slowik, J. G., Jaffrezo, J.-L., Baltensperger, U., Marchand, N.,

1 and Prévôt, A. S. H.: Organic aerosol source apportionment by offline-AMS over a full year in
2 Marseille, *Atmos. Chem. Phys. Discuss.*, 17, 8247-8268, 2017.

3 Bressi, M., Cavalli, F., Belis, C. A., Putaud, J.-P., Fröhlich, R., Martins dos Santos, S., Petralia, E.,
4 Prévôt, A. S. H., Berico, M., Malaguti, A., and Canonaco, F.: Variations in the chemical composition
5 of the submicron aerosol and in the sources of the organic fraction at a regional background site of the
6 Po Valley (Italy), *Atmos. Chem. Phys.*, 16, 12875-12896, <https://doi.org/10.5194/acp-16-12875-2016>,
7 2016.

8 Canagaratna, M. R., Jayne, J. T., Ghertner, D. A., Herndon, S., Shi, Q., Jimenez, J. L., Silva, P. J.,
9 Williams, P., Lanni, T., Drewnick, F., Demerjian, K. L., Kolb, C. E., Worsnop, D. R.: Chase studies
10 of particulate emissions from in-use New York City vehicles, *Aerosol Sci. Tech.* 38, 555-573, 2004.

11 Canonaco, F., Crippa, M., Slowik, J. G., Baltensperger, U., and Prévôt, A. S. H.: SoFi, an IGOR
12 based interface for the efficient use of the generalized multilinear engine (ME-2) for the source
13 apportionment: ME-2 application to aerosol mass spectrometer data, *Atmos. Meas. Tech.*, 6, 3649–
14 3661, [doi:10.5194/amt-6-3649-2013](https://doi.org/10.5194/amt-6-3649-2013), 2013.

15 Canonaco, F., Slowik, J. G., Baltensperger, U., and Prévôt, A. S. H.: Seasonal differences in
16 oxygenated organic aerosol composition: implications for emissions sources and factor analysis,
17 *Atmos. Chem. Phys.*, 15, 6993-7002, [doi:10.5194/acp-15-6993-2015](https://doi.org/10.5194/acp-15-6993-2015), 2015.

18 Chen, D. S., Cheng, S. Y., Liu, L., Chen, T., Guo, X. R.: An integrated MM5-CMAQ modeling
19 approach for assessing trans-boundary PM10 contribution to the host city of 2008 Olympic summer
20 games-Beijing, China, *Atmospheric Environment*, 41, 1237-1250, 2007.

21 Cohen, A. J., Brauer, M., Burnett, R., Anderson, H. R., Frostad, J., Estep, K., Balakrishnan, K.,
22 Brunekreef, B., Dandona, L., Dandona, R., Feigin, V., Freedman, G., Hubbell, B., Jobling, A., Kan,
23 H. D., Knibbs, L., Liu, Y., Martin, R., Morawska, L., Pope III, C. A., Shin, H., Straif, K., Shaddick,
24 G., Thomas, M., van Dingenen, R., van Donkelaar, A., Vos, T., Murray, C. J. L., Forouzanfar, M. H.:
25 Estimates and 25-year trends of the global burden of disease attributable to ambient air pollution: an
26 analysis of data from the Global Burden of Diseases Study 2015. *The Lancet* 389, 1907-1918, 2017.

1 Crippa, M., DeCarlo, P. F., Slowik, J. G., Mohr, C., Heringa, M. F., Chirico, R., Poulain, L., Freutel,
2 F., Sciare, J., Cozic, J., Di Marco, C. F., Elsasser, M., Nicolas, J. B., Marchand, N., Abidi, E.,
3 Wiedensohler, A., Drewnick, F., Schneider, J., Borrmann, S., Nemitz, E., Zimmermann, R., Jaffrezo,
4 J.-L., Prévôt, A. S. H., and Baltensperger, U.: Wintertime aerosol chemical composition and source
5 apportionment of the organic fraction in the metropolitan area of Paris, *Atmos. Chem. Phys.*, 13, 961-
6 981, doi:10.5194/acp-13-961-2013, 2013.

7 Crippa, M., Canonaco, F., Lanz, V. A., Äijälä, M., Allan, J. D., Carbone, S., Capes, G., Ceburnis, D.,
8 Dall'Osto, M., Day, D. A., DeCarlo, P. F., Ehn, M., Eriksson, A., Freney, E., Hildebrandt Ruiz, L.,
9 Hillamo, R., Jimenez, J. L., Junninen, H., Kiendler-Scharr, A., Kortelainen, A.-M., Kulmala, M.,
10 Laaksonen, A., Mensah, A. A., Mohr, C., Nemitz, E., O'Dowd, C., Ovadnevaite, J., Pandis, S. N.,
11 Petäjä, T., Poulain, L., Saarikoski, S., Sellegri, K., Swietlicki, E., Tiitta, P., Worsnop, D. R.,
12 Baltensperger, U., and Prévôt, A. S. H.: Organic aerosol components derived from 25 AMS data sets
13 across Europe using a consistent ME-2 based source apportionment approach, *Atmos. Chem. Phys.*,
14 14, 6159– 6176, doi:10.5194/acp-14-6159-2014, 2014.

15 Decarlo, P. F., Ulbrich, I. M., Crouse, J., De Foy, B., Dunlea, E. J., Aiken, A. C., Knapp, D.,
16 Weinheimer, A. J., Campos, T., Wennberg, P. O., Jimenez, J. L.: Investigation of the sources and
17 processing of organic aerosol over the Central Mexican Plateau from aircraft measurements during
18 MILAGRO, *Atmos. Chem. Phys.*, 10, 5257-5280, doi:10.5194/acp-10-5257-2010, 2010

19 Elser, M., Huang, R.-J., Wolf, R., Slowik, J. G., Wang, Q., Canonaco, F., Li, G., Bozzetti, C.,
20 Daellenbach, K. R., Huang, Y., Zhang, R., Li, Z., Cao, J., Baltensperger, U., El-Haddad, I., and
21 Prévôt, A. S. H.: New insights into PM_{2.5} chemical composition and sources in two major cities in
22 China during extreme haze events using aerosol mass spectrometry, *Atmos. Chem. Phys.*, 16, 3207-
23 3225, doi:10.5194/acp-16-3207-2016, 2016a.

24 Elser, M., Bozzetti, C., El-Haddad, I., Maasikmets, M., Teinmaa, E., Richter, R., Wolf, R., Slowik, J.
25 G., Baltensperger, U., and Prévôt, A. S. H.: Urban increments of gaseous and aerosol pollutants and
26 their sources using mobile aerosol mass spectrometry measurements, *Atmos. Chem. Phys.*, 16, 7117-
27 7134, doi:10.5194/acp-16-7117-2016, 2016b.

1 Ervens, B., Turpin, B. J., and Weber, R. J.: Secondary organic aerosol formation in cloud droplets and
2 aqueous particles (aqSOA): a review of laboratory, field and model studies, *Atmos. Chem. Phys.*, 11,
3 11069–11102, doi:10.5194/acp-11-11069-2011, 2011.

4 Fröhlich, R., Cubison, M. J., Slowik, J. G., Bukowiecki, N., Prévôt, A. S. H., Baltensperger, U.,
5 Schneider, J., Kimmel, J. R., Gonin, M., Rohner, U., Worsnop, D. R., and Jayne, J. T.: The ToF-
6 ACSM: a portable aerosol chemical speciation monitor with TOFMS detection, *Atmos. Meas. Tech.*,
7 6, 3225-3241, <https://doi.org/10.5194/amt-6-3225-2013>, 2013.

8 Fröhlich, R., Crenn, V., Setyan, A., Belis, C. A., Canonaco, F., Favez, O., Riffault, V., Slowik, J. G.,
9 Aas, W., Aijälä, M., Alastuey, A., Artiñano, B., Bonnaire, N., Bozzetti, C., Bressi, M., Carbone, C.,
10 Coz, E., Croteau, P. L., Cubison, M. J., Esser-Gietl, J. K., Green, D. C., Gros, V., Heikkinen, L.,
11 Herrmann, H., Jayne, J. T., Lunder, C. R., Minguillón, M. C., Mocnik, G., O’Dowd, C. D.,
12 Ovadnevaite, J., Petralia, E., Poulain, L., Priestman, M., Ripoll, A., Sarda-Estève, R., Wiedensohler,
13 A., Baltensperger, U., Sciare, J., and Prévôt, A. S. H.: ACTRIS ACSM intercomparison–Part 2:
14 Intercomparison of ME-2 organic source apportionment results from 15 individual, co-located aerosol
15 mass spectrometers, *Atmos. Meas. Tech.*, 8, 2555–2576, doi:10.5194/amt- 8-2555-2015, 2015a.

16 Fröhlich, R., Cubison, M. J., Slowik, J. G., Bukowiecki, N., Canonaco, F., Croteau, P. L., Gysel, M.,
17 Henne, S., Herrmann, E., Jayne, J. T., Steinbacher, M., Worsnop, D. R., Baltensperger, U., and
18 Prévôt, A. S. H.: Fourteen months of on-line measurements of the non-refractory submicron aerosol at
19 the Jungfraujoch (3580 m a.s.l.) – chemical composition, origins and organic aerosol sources, *Atmos.*
20 *Chem. Phys.*, 15, 11373-11398, doi:10.5194/acp-15-11373-2015, 2015b.

21 Ge, X., Zhang, Q., Sun, Y. L., Ruehl, C. R., and Setyan, A.: Effect of aqueous-phase processing on
22 aerosol chemistry and size distributions in Fresno, California, during wintertime, *Environmental*
23 *Chemistry*, 9, 221–235, doi:10.1071/EN11168, 2012.

24 Guo, S., Hu, M., Wang, Z. B., Slanina, J., and Zhao, Y. L.: Size resolved aerosol water-soluble ionic
25 compositions in the summer of Beijing: implication of regional secondary formation, *Atmos. Chem.*
26 *Phys.*, 10, 947–959, doi:10.5194/acp-10-947-2010, 2010.

1 He, L.-Y., Lin, Y., Huang, X.-F., Guo, S., Xue, L., Su, Q., Luan, S.- J., and Zhang, Y.-H.:
2 Characterization of high-resolution aerosol mass spectra of primary organic aerosol emissions from
3 Chinese cooking and biomass burning, *Atmos. Chem. Phys.*, 10, 11535– 11543, doi:10.5194/acp-10-
4 11535-2010, 2010.

5 He, L.-Y., Huang, X.-F., Xue, L., Hu, M., Lin, Y., Zheng, J., Zhang, R., and Zhang, Y.-H.: Submicron
6 aerosol analysis and organic source apportionment in an urban atmosphere in Pearl River Delta of
7 China using high-resolution aerosol mass spectrometry, *J. Geophys. Res.*, 116, D12304,
8 doi:10.1029/2010JD014566, 2011.

9 Hu, W., Hu, M., Hu, W., Jimenez, J. L., Yuan, B., Chen, W., Wang, M., Wu, Y., Chen, C., Wang, Z.,
10 Peng, J., Zeng, L., and Shao, M.: Chemical composition, sources and aging process of submicron
11 aerosols in Beijing: contrast between summer and winter, *J. Geophys. Res.*, 121, 1955–1977,
12 doi:10.1002/2015JD024020, 2016a.

13 Hu, W., Hu, M., Hu, W.-W., Niu, H., Zheng, J., Wu, Y., Chen, W., Chen, C., Li, L., Shao, M., Xie,
14 S., and Zhang, Y.: Characterization of submicron aerosols influenced by biomass burning at a site in
15 the Sichuan Basin, southwestern China, *Atmos. Chem. Phys.*, 16, 13213-13230, doi:10.5194/acp-16-
16 13213-2016, 2016b.

17 Huang, R. J., Zhang, Y., Bozzetti, C., Ho, K. F., Cao, J. J., Han, U., Daellenbach, K. R., Slowik, J. G.,
18 Platt, S. M., Canonaco, F., Zotter, P., Wolf, R., Pieber, S. M., Bruns, E. A., Crippa, M., Ciarelli, G.,
19 Piazzalunga, A., Schwikowski, M., Abbaszade, G., Schnelle-Kreis, J., Zimmermann, R., An, Z.,
20 Szidat, S., Baltensperger, U., El Haddad, I. and Prévôt, A. S. H.: High secondary aerosol contribution
21 to particulate pollution during haze events in China, *Nature*, 514, 218–222, 2014.

22 Huang, X.-F., He, L.-Y., Xue, L., Sun, T.-L., Zeng, L.-W., Gong, Z.-H., Hu, M., and Zhu, T.: Highly
23 time-resolved chemical characterization of atmospheric fine particles during 2010 Shanghai World
24 Expo, *Atmos. Chem. Phys.*, 12, 4897-4907, doi:10.5194/acp-12-4897-2012, 2012.

25 Huang, X.-F., Xue, L., Tian, X.-D., Shao, W.-W., Sun, T.-L., Gong, Z.-H., Ju, W.-W., Jiang, B., Hu,
26 M., and He, L.-Y.: Highly time-resolved carbonaceous aerosol characterization in yangtze river delta

1 of china: Composition, mixing state and secondary formation, *Atmos. Environ.*, 64, 200–207,
2 doi:10.1016/j.atmosenv.2012.09.059, 2013.

3 Jiang, Q., Sun, Y. L., Wang, Z., and Yin, Y.: Aerosol composition and sources during the Chinese
4 Spring Festival: fireworks, secondary aerosol, and holiday effects, *Atmos. Chem. Phys.*, 15, 6023–
5 6034, doi:10.5194/acp-15-6023-2015, 2015.

6 Jimenez, J. L., Canagaratna, M. R., Donahue, N. M., Prévôt, A. S. H., Zhang, Q., Kroll, J. H.,
7 DeCarlo, P. F., Allan, J. D., Coe, H., Ng, N. L., Aiken, A. C., Docherty, K. S., Ulbrich, I. M.,
8 Grieshop, A. P., Robinson, A. L., Duplissy, J., Smith, J. D., Wilson, K. R., Lanz, V. A., Hueglin, C.,
9 Sun, Y. L., Tian, J., Laaksonen, A., Raatikainen, T., Rautiainen, J., Vaattovaara, P., Ehn, M.,
10 Kulmala, M., Tomlinson, J. M., Collins, D. R., Cubison, M. J., E, Dunlea, J., Huffman, J. A., Onasch,
11 T. B., Alfarra, M. R., Williams, P. I., Bower, K., Kondo, Y., Schneider, J., Drewnick, F., Borrmann,
12 S., Weimer, S., Demerjian, K., Salcedo, D., Cottrell, L., Griffin, R., Takami, A., Miyoshi, T.,
13 Hatakeyama, S., Shimono, A., Sun, J. Y., Zhang, Y. M., Dzepina, K., Kimmel, J. R., Sueper, D.,
14 Jayne, J. T., Herndon, S. C., Trimborn, A. M., Williams, L. R., Wood, E. C., Middlebrook, A. M.,
15 Kolb, C. E., Baltensperger, U., and Worsnop, D. R.: Evolution of organic aerosols in the atmosphere,
16 *Science*, 326, 1525–1529, 2009.

17 Lang, J.L., Cheng, S.Y., Li, J.B., Chen, D.S., Zhou, Y., Wei, X., Han, L.H., and Wang, H.Y.: A
18 monitoring and modeling study to investigate regional transport and characteristics of PM2.5
19 pollution, *Aerosol Air Qual. Res.*, 13, 943–956, 2013.

20 Lanz, V. A., Alfarra, M. R., Baltensperger, U., Buchmann, B., Hueglin, C., and Prévôt, A. S. H.:
21 Source apportionment of submicron organic aerosols at an urban site by factor analytical modelling of
22 aerosol mass spectra, *Atmos. Chem. Phys.*, 7, 1503–1522, doi:10.5194/acp-7-1503-2007, 2007.

23 Li, H., Zhang, Q., Zhang, Q., Chen, C., Wang, L., Wei, Z., Zhou, S., Parworth, C., Zheng, B.,
24 Canonaco, F., Prévôt, A. S. H., Chen, P., Zhang, H., Wallington, T. J., and He, K.: Wintertime aerosol
25 chemistry and haze evolution in an extremely polluted city of North China Plain: significant
26 contribution from coal and biomass combustions, *Atmos. Chem. Phys.*, 17, 4751–4768,
27 doi:10.5194/acp-2016-1058, 2017.

1 Li, P., Yan, R., Yu, S., Wang, S., Liu, W., and Bao, H.: Reinstatement of regional transport of PM_{2.5} as a
2 major cause of severe haze in Beijing, *P. Natl. Acad. Sci.*, 112, E2739–E2740,
3 doi:10.1073/pnas.1502596112, 2015a.

4 Li, Y. J., Lee, B. Y. L., Yu, J. Z., Ng, N. L., and Chan, C. K.: Evaluating the degree of oxygenation of
5 organic aerosol during foggy and hazy days in Hong Kong using high-resolution time-of-flight
6 aerosol mass spectrometry (HR-ToF-AMS), *Atmos. Chem. Phys.*, 13, 8739–8753, doi:10.5194/acp-
7 13-8739-2013, 2013

8 Li, Y. J., Lee, B. P., Su, L., Fung, J. C. H., and Chan, C. K.: Seasonal characteristics of fine
9 particulate matter (PM) based on high-resolution time-of-flight aerosol mass spectrometric (HR-ToF-
10 AMS) measurements at the HKUST Supersite in Hong Kong, *Atmos. Chem. Phys.*, 15, 37–53,
11 doi:10.5194/acp-15-37-2015, 2015b.

12 Middlebrook, A. M., Bahreini, R., Jimenez, J. L., and Canagaratna, M. R.: Evaluation of
13 Composition-Dependent Collection Efficiencies for the Aerodyne Aerosol Mass Spectrometer using
14 Field Data, *Aerosol Sci. Tech.*, 46, 258–271, 2012.

15 Minguillón, M. C., Ripoll, A., Pérez, N., Prévôt, A. S. H., Canonaco, F., Querol, X., and Alastuey, A.:
16 Chemical characterization of submicron regional background aerosols in the western Mediterranean
17 using an Aerosol Chemical Speciation Monitor, *Atmos. Chem. Phys.*, 15, 6379–6391,
18 doi:10.5194/acp-15-6379-2015, 2015.

19 Mohr, C., Huffman, J. A., Cubison, M. J., Aiken, A. C., Docherty, K. S., Kimmel, J. R., Ulbrich, I.
20 M., Hannigan, M., and Jimenez, J. L.: Characterization of primary organic aerosol emissions from
21 meat cooking, trash burning, and motor vehicles with High-Resolution Aerosol Mass Spectrometry
22 and comparison with ambient and chamber observations, *Environ. Sci. Technol.*, 43, 2443–2449,
23 doi:10.1021/es8011518, 2009.

24 Mohr, C., DeCarlo, P. F., Heringa, M. F., Chirico, R., Slowik, J. G., Richter, R., Reche, C., Alastuey,
25 A., Querol, X., Seco, R., Peñuelas, J., Jiménez, J. L., Crippa, M., Zimmermann, R., Baltensperger,
26 U., and Prévôt, A. S. H.: Identification and quantification of organic aerosol from cooking and other

1 sources in Barcelona using aerosol mass spectrometer data, *Atmos. Chem. Phys.*, 12, 1649–1665,
2 doi:10.5194/acp-12-1649-2012, 2012.

3 Ng, N. L., Canagaratna, M. R., Zhang, Q., Jimenez, J. L., Tian, J., Ulbrich, I. M., Kroll, J. H.,
4 Docherty, K. S., Chhabra, P. S., Bahreini, R., Murphy, S. M., Seinfeld, J. H., Hildebrandt, L.,
5 Donahue, N. M., DeCarlo, P. F., Lanz, V. A., Prévôt, A. S. H., Dinar, E., Rudich, Y., and Worsnop,
6 D. R.: Organic aerosol components observed in Northern Hemispheric datasets from Aerosol Mass
7 Spectrometry, *Atmos. Chem. Phys.*, 10, 4625-4641, doi:10.5194/acp-10-4625-2010, 2010.

8 Ng, N. L., Herndon, S. C., Trimborn, A., Canagaratna, M. R., Croteau, P. L., Onasch, T. B., Sueper,
9 D., Worsnop, D. R., Zhang, Q., Sun, Y. L., and Jayne, J. T.: An Aerosol Chemical Speciation Monitor
10 (ACSM) for Routine Monitoring of the Composition and Mass Concentrations of Ambient Aerosol,
11 *Aerosol Sci. Tech.*, 45, 770–784, 2011a.

12 Ng, N. L., Canagaratna, M. R., Jimenez, J. L., Zhang, Q., Ulbrich, I. M., and Worsnop, D. R.: Real-
13 time methods for estimating organic component mass concentrations from aerosol mass spectrometer
14 data, *Environ. Sci. Technol.*, 45, 910–916, 2011b.

15 Paatero, P., and Tapper, U., Positive Matrix Factorization: A Non-Negative Factor Model with
16 Optimal Utilization of Error Estimates of Data Values, *Environmetrics*, 5, 111–126, doi:
17 10.1002/env.3170050203, 1994.

18 Petit, J.-E., Favez, O., Sciare, J., Crenn, V., Sarda-Estève, R., Bonnaire, N., Močnik, G., Dupont, J.-
19 C., Haeffelin, M., and Leoz-Garziandia, E.: Two years of near real-time chemical composition of
20 submicron aerosols in the region of Paris using an Aerosol Chemical Speciation Monitor (ACSM) and
21 a multi-wavelength Aethalometer, *Atmos. Chem. Phys.*, 15, 2985-3005, doi:10.5194/acp-15-2985-
22 2015, 2015.

23 Ripoll, A., Minguillón, M. C., Pey, J., Jimenez, J. L., Day, D. A., Sosedova, Y., Canonaco, F., Prévôt,
24 A. S. H., Querol, X., and Alastuey, A.: Long-term real-time chemical characterization of submicron
25 aerosols at Montsec (southern Pyrenees, 1570 m a.s.l.), *Atmos. Chem. Phys.*, 15, 2935-2951,
26 doi:10.5194/acp-15-2935-2015, 2015.

1 Reyes-Villegas, E., Green, D. C., Priestman, M., Canonaco, F., Coe, H., Prévôt, A. S. H., and Allan, J.
2 D.: Organic aerosol source apportionment in London 2013 with ME-2: exploring the solution space
3 with annual and seasonal analysis, *Atmos. Chem. Phys.*, 16, 15545-15559, doi:10.5194/acp-16-
4 15545-2016, 2016.

5 Schlag, P., Kiendler-Scharr, A., Blom, M. J., Canonaco, F., Henzing, J. S., Moerman, M., Prévôt, A.
6 S. H., and Holzinger, R.: Aerosol source apportionment from 1-year measurements at the CESAR
7 tower in Cabauw, the Netherlands, *Atmos. Chem. Phys.*, 16, 8831-8847, <https://doi.org/10.5194/acp->
8 16-8831-2016, 2016.

9 Schneider, J., Weimer, S., Drewnick, F., Borrmann, S., Helas, G. Gwaze, P., Schmid, O., Andreae, M.
10 O., and Kirchner, U.: Mass spectrometric analysis and aerodynamic properties of various types of
11 combustion-related aerosol particles, *Int. J. Mass Spectrom.*, 258, 37–49,
12 doi:10.1016/j.ijms.2006.07.008, 2006.

13 Sun, Y. L., Wang, Z. F., Fu, P. Q., Yang, T., Jiang, Q., Dong, H. B., Li, J., and Jia, J. J.: Aerosol
14 composition, sources and processes during wintertime in Beijing, China, *Atmos. Chem. Phys.*, 13,
15 4577–4592, doi:10.5194/acp-13-4577-2013, 2013.

16 Sun, Y. L., Jiang, Q., Wang, Z., Fu, P., Li, J., Yang, T., and Yin, Y.: Investigation of the sources and
17 evolution processes of severe haze pollution in Beijing in January 2013, *J. Geophys. Res.*, 119, 4380–
18 4398, doi:10.1002/2014JD021641, 2014.

19 Sun, Y. L., Wang, Z. F., Du, W., Zhang, Q., Wang, Q. Q., Fu, P. Q., Pan, X. L., Li, J., Jayne, J., and
20 Worsnop, D. R.: Long-term real-time measurements of aerosol particle composition in Beijing, China:
21 seasonal variations, meteorological effects, and source analysis, *Atmos. Chem. Phys.*, 15, 10149-
22 10165, doi:10.5194/acp-15-10149-2015, 2015.

23 Sun, Y., Du, W., Fu, P., Wang, Q., Li, J., Ge, X., Zhang, Q., Zhu, C., Ren, L., Xu, W., Zhao, J., Han,
24 T., Worsnop, D. R., and Wang, Z.: Primary and secondary aerosols in Beijing in winter: sources,
25 variations and processes, *Atmos. Chem. Phys.*, 16, 8309-8329, doi:10.5194/acp-16-8309-2016, 2016.

1 Tie, X., Huang, R. J., Cao, J. J., Zhang, Q., Cheng, Y. F., Su, H., Chang, D., Pöschl, U., Hoffmann,
2 T., Dusek, U., Li, G. H., Worsnop, D. R., O'Dowd, C. D.: Severe pollution in China amplified by
3 atmospheric moisture, *Sci. Rep.*, 7: 15760, DOI:10.1038/s41598-017-15909-1, 2017

4 Ulbrich, I. M., Canagaratna, M. R., Zhang, Q., Worsnop, D. R., and Jimenez, J. L.: Interpretation of
5 organic components from Positive Matrix Factorization of aerosol mass spectrometric data, *Atmos.*
6 *Chem. Phys.*, 9, 2891-2918, doi:10.5194/acp-9-2891-2009, 2009.

7 Wang, G., Zhang, R., Gomez, M.E., Yang, L., Levy Zamora, M., Hu, M., Lin, Y., Peng, J., Guo, S.,
8 Meng, J., Li, J., Cheng, C., Hu, T., Ren, Y., Wang, Y., Gao, J., Cao, J., An, Z., Zhou, W., Li, G.,
9 Wang, J., Tian, P., Marrero-Ortiz, W., Secrest, J., Du, Z., Zheng, J., Shang, D., Zeng, L., Shao, M.,
10 Wang, W., Huang, Y., Wang, Y., Zhu, Y., Li, Y., Hu, J., Pan, B., Cai, L., Cheng, Y., Ji, Y., Zhang, F.,
11 Rosenfeld, D., Liss, P.S., Duce, R.A., Kolb, C.E., and Molina, M.J., Persistent sulfate formation from
12 London fog to Chinese haze, *Proc. Natl. Acad. Sci.*, 113, 13630-13635, 2016.

13 Wang, Q, Sun Y, Jiang Q, et al. Chemical composition of aerosol particles and light extinction
14 apportionment before and during the heating season in Beijing, China, *J. Geophys. Res. Atmos.*, 120,
15 12708-12722, 2015.

16 Wang, Y. C., Huang, R. J., Ni, H. Y., Chen, Y., Wang, Q. Y., Li, G. H., Tie, X. X., Shen, Z. X.,
17 Huang, Y., Liu, S. X., Dong, W. M., Xue, P., Frohlich, R., Canonaco, F., Elser, M., Daellenbach, K.
18 R., Bozzetti, C., El Haddad, I., Prevot, A. S. H.: Chemical composition, sources and secondary
19 processes of aerosols in Baoji city of northwest China, *Atmos. Environ.*, 158, 128-137, 2017.

20 Xu, X., Barsha, N.A.F. and Li, J.: Analyzing Regional Influence of Particulate Matter on the City of
21 Beijing, China, *Aerosol Air Qual. Res.*, 8, 78-93, 2008.

22 Xu, J., Zhang, Q., Chen, M., Ge, X., Ren, J., and Qin, D.: Chemical composition, sources, and
23 processes of urban aerosols during summertime in northwest China: insights from high-resolution
24 aerosol mass spectrometry, *Atmos. Chem. Phys.*, 14, 12593-12611, doi:10.5194/acp-14-12593-2014,
25 2014.

1 Xu, J., Shi, J., Zhang, Q., Ge, X., Canonaco, F., Prévôt, A. S. H., Vonwiller, M., Szidat, S., Ge, J.,
2 Ma, J., An, Y., Kang, S., and Qin, D.: Wintertime organic and inorganic aerosols in Lanzhou, China:
3 sources, processes, and comparison with the results during summer, *Atmos. Chem. Phys.*, 16, 14937-
4 14957, doi:10.5194/acp-16-14937-2016, 2016.

5 Xu, W. Q., Sun, Y. L., Chen, C., Du, W., Han, T. T., Wang, Q. Q., Fu, P. Q., Wang, Z. F., Zhao, X. J.,
6 Zhou, L. B., Ji, D. S., Wang, P. C., and Worsnop, D. R.: Aerosol composition, oxidation properties,
7 and sources in Beijing: results from the 2014 Asia-Pacific Economic Cooperation summit study,
8 *Atmos. Chem. Phys.*, 15, 13681-13698, doi:10.5194/acp-15-13681-2015, 2015.

9 Zhang, J. P., Zhu, T., Zhang, Q. H., Li, C. C., Shu, H. L., Ying, Y., Dai, Z. P., Wang, X., Liu, X. Y.,
10 Liang, A. M., Shen, H. X., and Yi, B. Q.: The impact of circulation patterns on regional transport
11 pathways and air quality over Beijing and its surroundings, *Atmos. Chem. Phys.*, 12, 5031–5053,
12 doi:10.5194/acp-12-5031-2012, 2012.

13 Zhang, R. Y., Wang, G. H., Guo, S., Zamora, M. L., Ying, Q., Lin, Y., Wang, W., Hu, M., and Wang,
14 Y.: Formation of urban fine particulate matter, *Chem. Rev.*, 115, 3803–3855,
15 doi:10.1021/acs.chemrev.5b00067, 2015a.

16 Zhang, Y. J., Tang, L. L., Wang, Z., Yu, H. X., Sun, Y. L., Liu, D., Qin, W., Canonaco, F., Prévôt, A.
17 S. H., Zhang, H. L., and Zhou, H. C.: Insights into characteristics, sources, and evolution of
18 submicron aerosols during harvest seasons in the Yangtze River delta region, China, *Atmos. Chem.*
19 *Phys.*, 15, 1331-1349, doi:10.5194/acp-15-1331-2015, 2015b.

20 Zhang, Y. J., Tang, L. L., Yu, H. X., Wang, Z., Sun, Y.L., Qin, W., Chen, W. T., Chen, C. H., Ding,
21 A. J., Wu, J., Ge, S., Chen, C., and Zhou, H. C.: Chemical composition, sources and evolution
22 processes of aerosol at an urban site in Yangtze River Delta, China during wintertime, *Atmos.*
23 *Environ.*, 123, 339-349, 2015c.

24 Zhao, P., Dong, F., Yang, Y., He, D., Zhao, X., Zhang, W., Yao, Q., and Liu, H.: Characteristics of
25 carbonaceous aerosol in the region of Beijing, Tianjin, and Hebei, China, *Atmos. Environ.*, 71, 389–
26 398, 2013a.

1 Zhao, P. S., Dong, F., He, D., Zhao, X. J., Zhang, X. L., Zhang, W. Z., Yao, Q., and Liu, H. Y.:
2 Characteristics of concentrations and chemical compositions for PM_{2.5} in the region of Beijing,
3 Tianjin, and Hebei, China, *Atmos. Chem. Phys.*, 13, 4631–4644, doi:10.5194/acp-13-4631-2013,
4 2013b.

5 Zhou, W., Jiang, J., Duan, L., and Hao, J.: Evolution of submicron organic aerosols during a complete
6 residential coal combustion process, *Environ. Sci. Technol.*, 50, 7861–7869, 2016.

7 Zhu, Q., Huang, X.-F., Cao, L.-M., Wei, L.-T., Zhang, B., He, L.-Y., Elser, M., Canonaco, F., Slowik,
8 J. G., Bozzetti, C., El-Haddad, I., and Prévôt, A. S. H.: Improved source apportionment of organic
9 aerosols in complex urban air pollution using the multilinear engine (ME-2), *Atmos. Meas. Tech.*, 11,
10 1049-1060, <https://doi.org/10.5194/amt-11-1049-2018>, 2018.

11

12

13

14

15

16

17

18

19

20

21

22

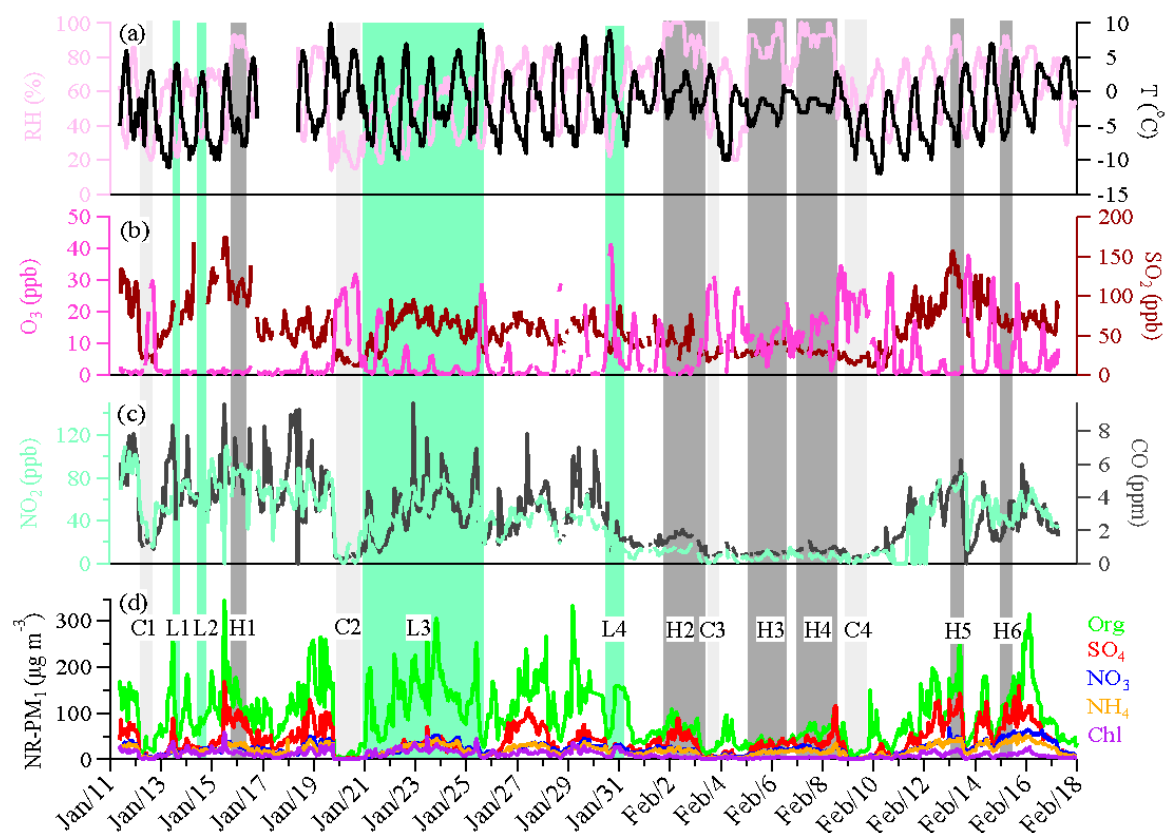
23

1 Table 1. The fine PM mass concentrations and fractional contribution of different composition in
 2 different locations.

City	Season	NR-PM ₁ ($\mu\text{g m}^{-3}$)	OA %	SO ₄ ²⁻ %	NO ₃ ⁻ %	NH ₄ ⁺ %	Cl ⁻ %	Ref.
Beijing	Winter, 2010	60	54	14	11	12	9	Hu et al., 2016a
Beijing	Winter, 2011	59	51	13	17	14	5	Sun et al., 2015
Beijing	Winter, 2012	66.8	52	14	16	13	5	Sun et al., 2013
Beijing	Winter, 2012	79	52	17	14	10	7	Wang et al., 2015
Beijing	Winter, 2013	77	50	19	16	12	3	Sun et al., 2014
Beijing	Winter, 2013	13.0	52	17	14	10	7	Jiang et al., 2015
Beijing	Winter, 2013	64	60	15	11	8	6	Sun et al., 2016
Beijing	Winter, 2014	75 ^a	56	16	10	7	11	Elser et al., 2016
Beijing	Summer, 2011	80	32	28	21	17	2	Hu et al., 2016a
Beijing	Summer, 2012	52	41	14	25	17	3	Sun et al., 2015
Lanzhou	Winter, 2014	57.3	55	13	18	11	3	Xu et al., 2016
Lanzhou	Summer,	24	53	18	11	13	5	Xu et al., 2014

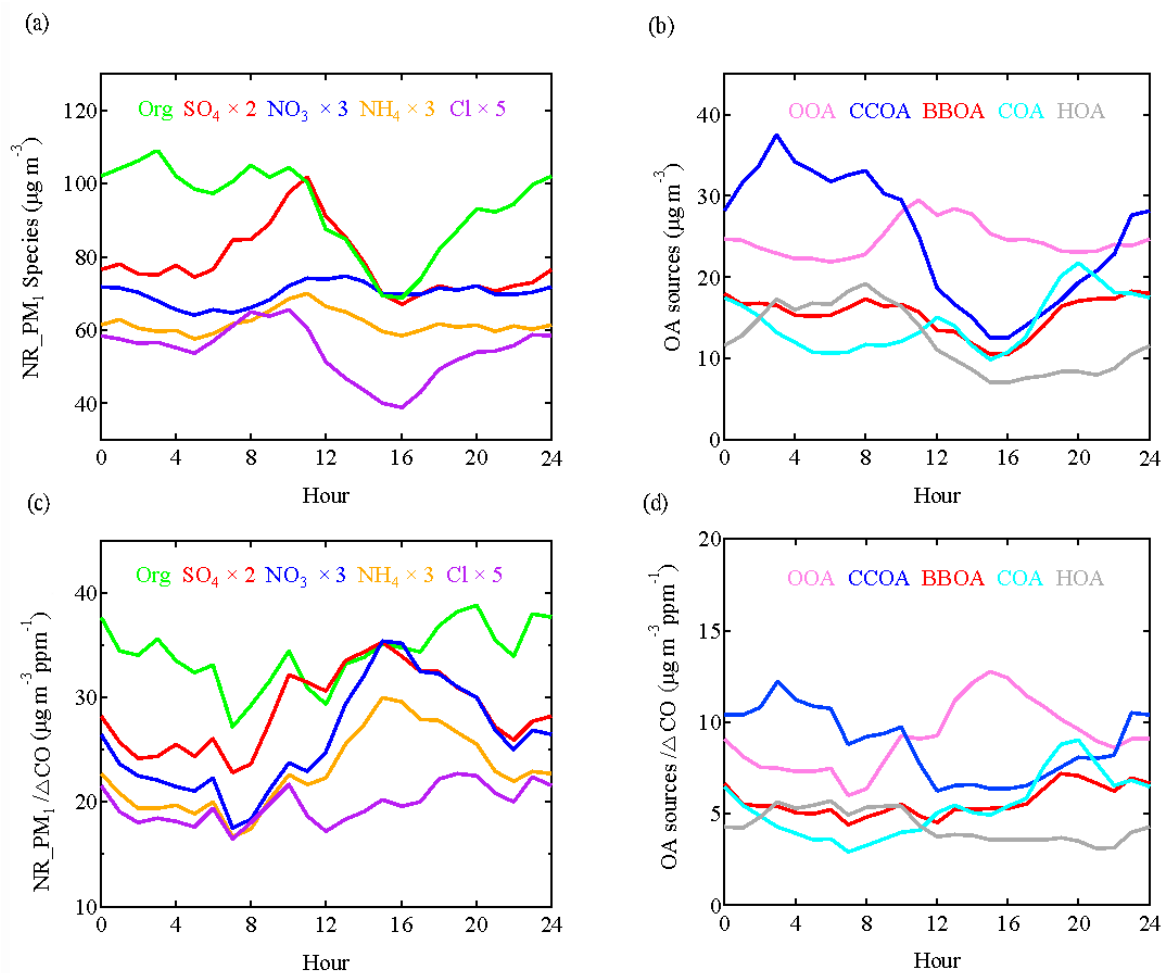
	2012								
Ziyang	Winter, 2012	60	40	24	15	17	4	Hu et al., 2016b	
Handan	Winter, 2015	178	47	16	15	13	9	Li et al., 2017	
Shenzhen	Autumn, 2009	38.3	46	29	12	11	2	He et al., 2011	
Shanghai	Summer, 2010	27	31	36	17	14	2	Huang et al., 2012	
Nanjing	Summer, 2013	36.8	42	14	24	19	1	Zhang et al., 2015b	
Hong Kong	Winter, 2012	14.5	33	40	10	16	1	Li et al., 2015b	
Hong Kong	Summer, 2011	8.7	26	56	3	15	0.1	Li et al., 2015b	
Paris	Winter, 2010	16.7	35	16	33	15	1	Crippa et al., 2013	
Fresno, California	Winter, 2010	11.8	67	3	20	8	2	Ge et al., 2012	
Shijiazhuang	Winter, 2014	178	50	21	12	11	6	This study	

1 ^aNR-PM_{2.5}



1
 2 **Fig. 1** Time series of relative humidity and temperature(a), O₃ and SO₂ (b), NO₂ and CO (c),
 3 and the NR-PM₁ species (d) during the observation period. 6 high-RH (>80%) polluted episodes
 4 (H1-H6), 4 low-RH (<60%) polluted episodes (L1-L4), and 4 clean episodes (C1-C4) are marked
 5 for further discussion.

6
 7

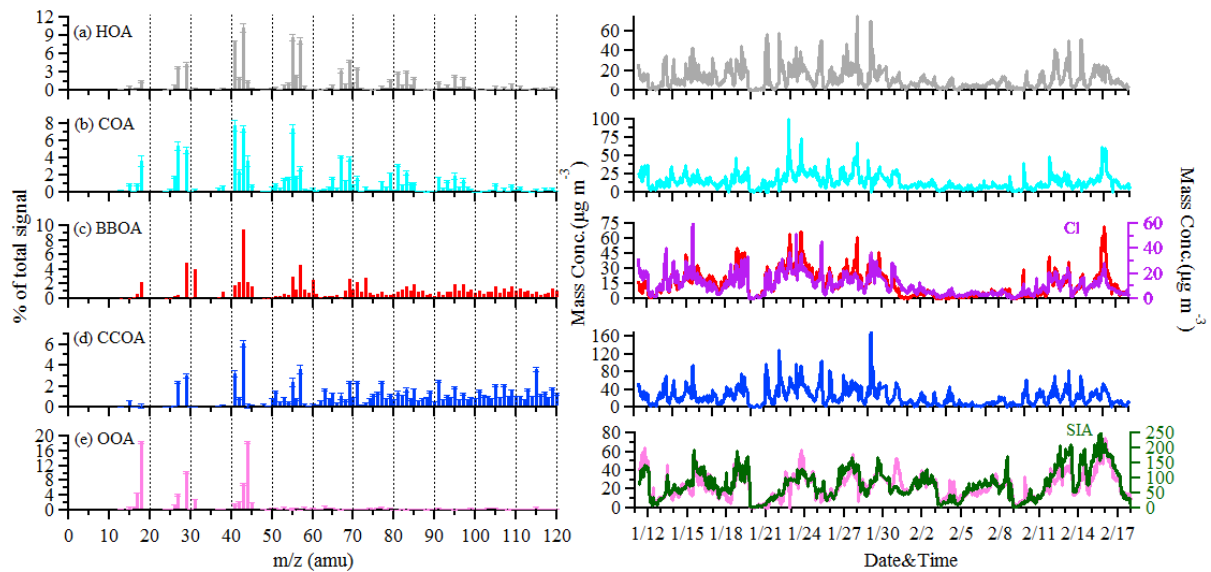


1

2 **Fig. 2. Diurnal variations of NR-PM₁ composition (a), OA sources (b), NR-PM₁ species/ΔCO (c)**
 3 **and OA sources/ΔCO (d).**

4

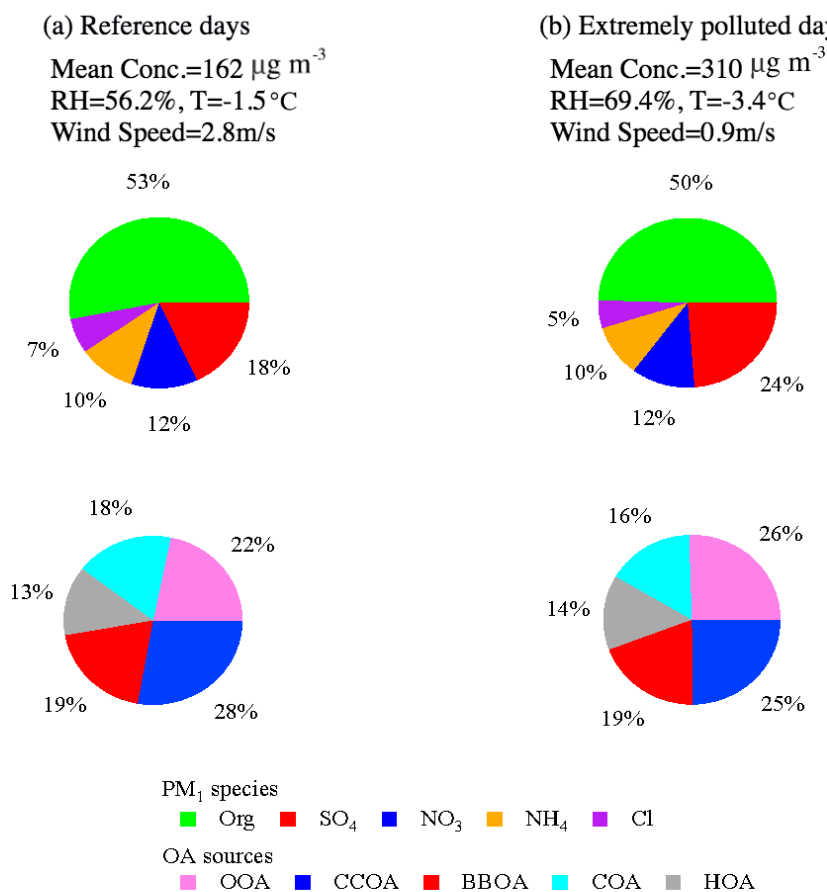
5



1

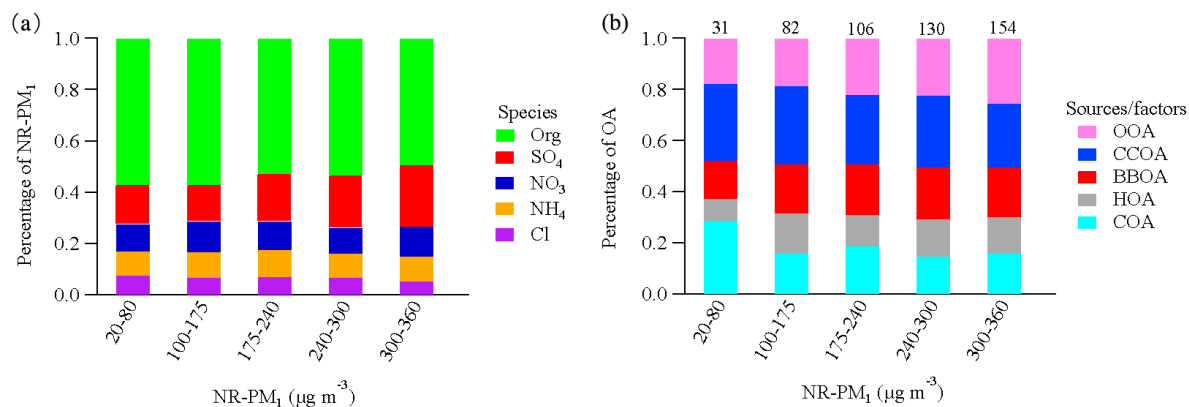
2 **Fig. 3** Mass spectrums (left) and time series (right) of five OA sources. Error bars of mass
 3 spectrums represent the standard deviation of each m/z over all accepted solutions.

4



1
 2
 3
 4
 5
 6
 7

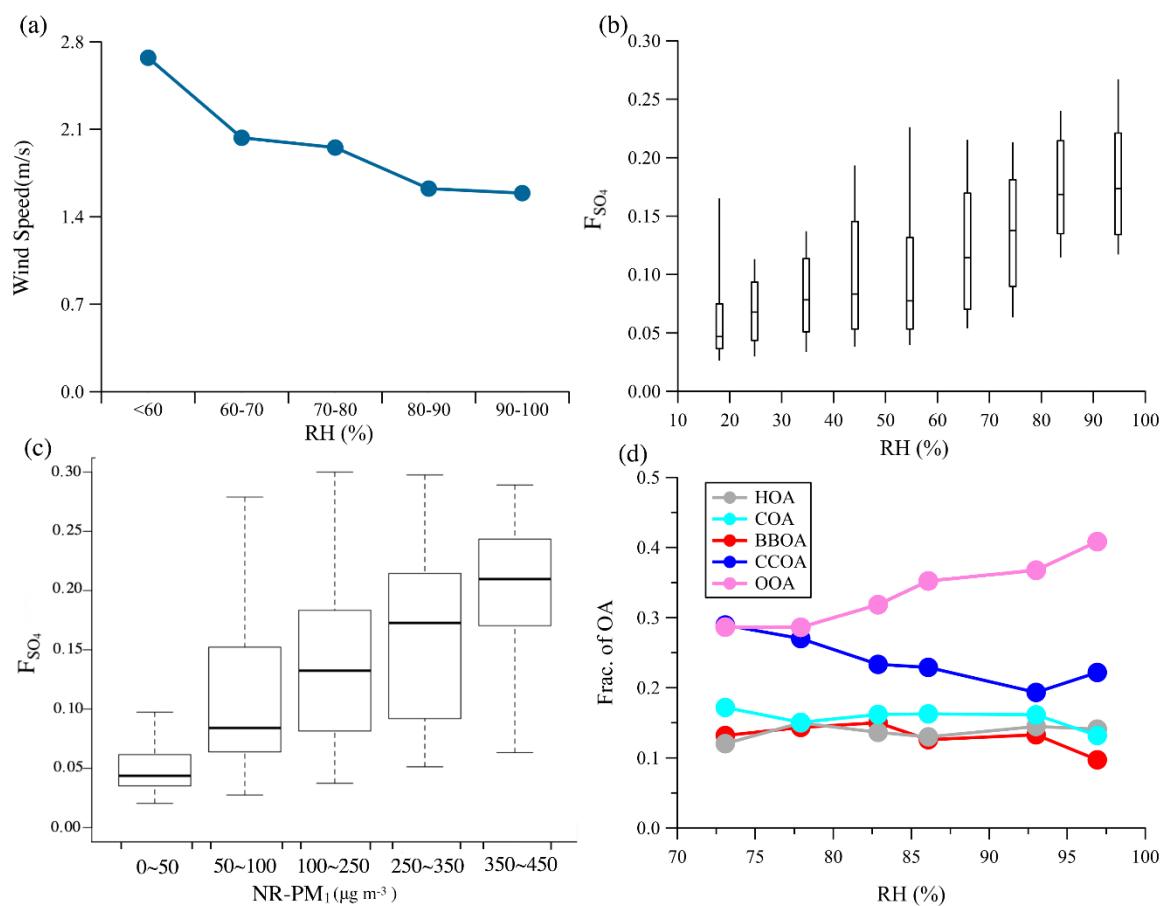
Fig. 4. Relative contributions of NR-PM₁ species and OA sources (OOA, CCOA, BBOA, COA and HOA) in reference days (a) and extremely polluted days (b). Extremely polluted days are defined as the daily average mass concentration of NR-PM₁ higher than the 75th percentile (237.3 $\mu\text{g m}^{-3}$) and the rest refers to the reference days. Data in the Spring Festival is excluded to eliminate the influence from a change of emission patterns in the holiday.



1

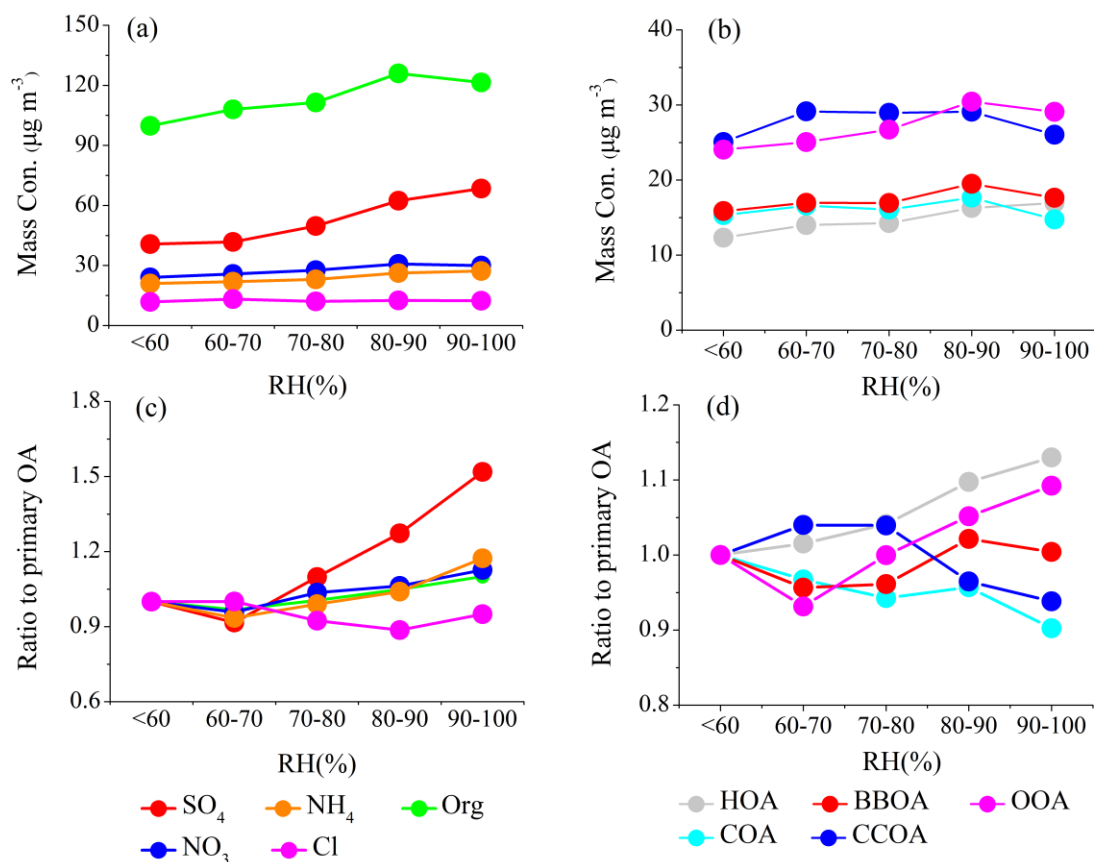
2 **Fig. 5. Relative contributions of NR-PM₁ species (a) and OA sources (b) as a function of daily**
 3 **average NR-PM₁ mass concentrations. The numbers above the bars refer to the OA mass**
 4 **concentration (µg m⁻³). Data in the Spring Festival is excluded to eliminate the influence from**
 5 **the change of emission patterns in the holiday.**

6



1

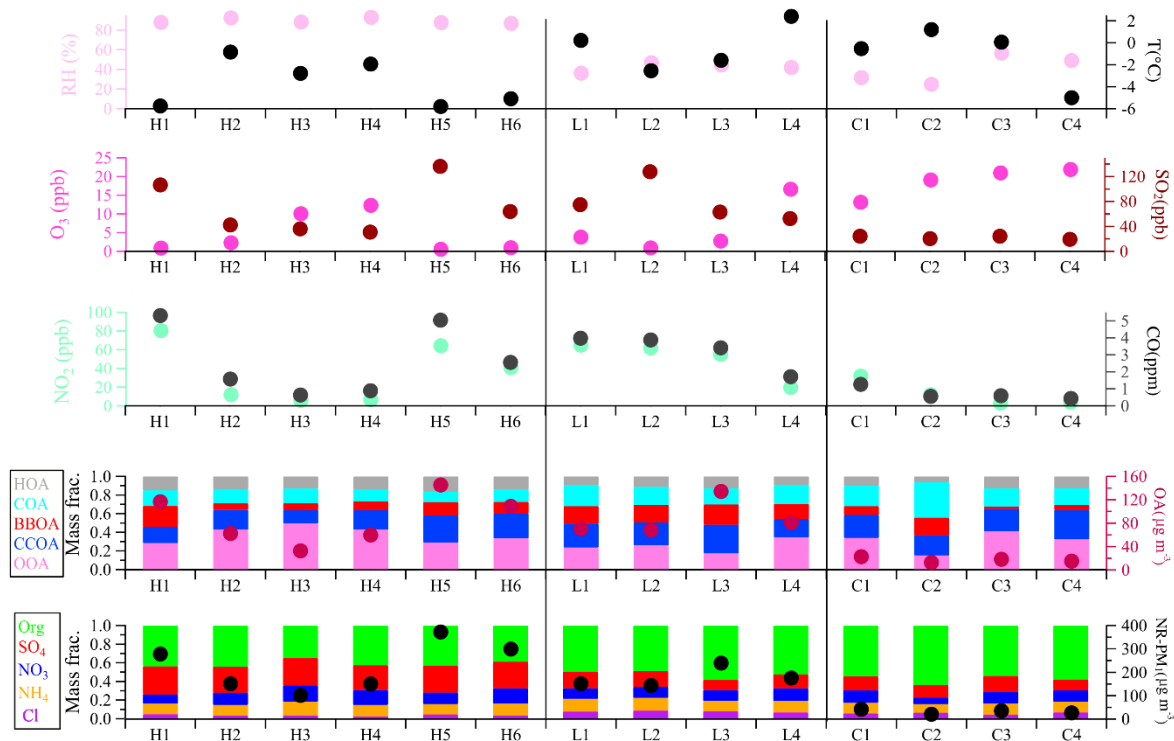
2 **Fig. 6.** Variations of wind speed as a function of RH (a), F_{SO_4} as a function of RH (b) and of the
 3 NR- PM_{10} mass concentrations (c), and the mass fraction of organic as a function of RH (d).



1

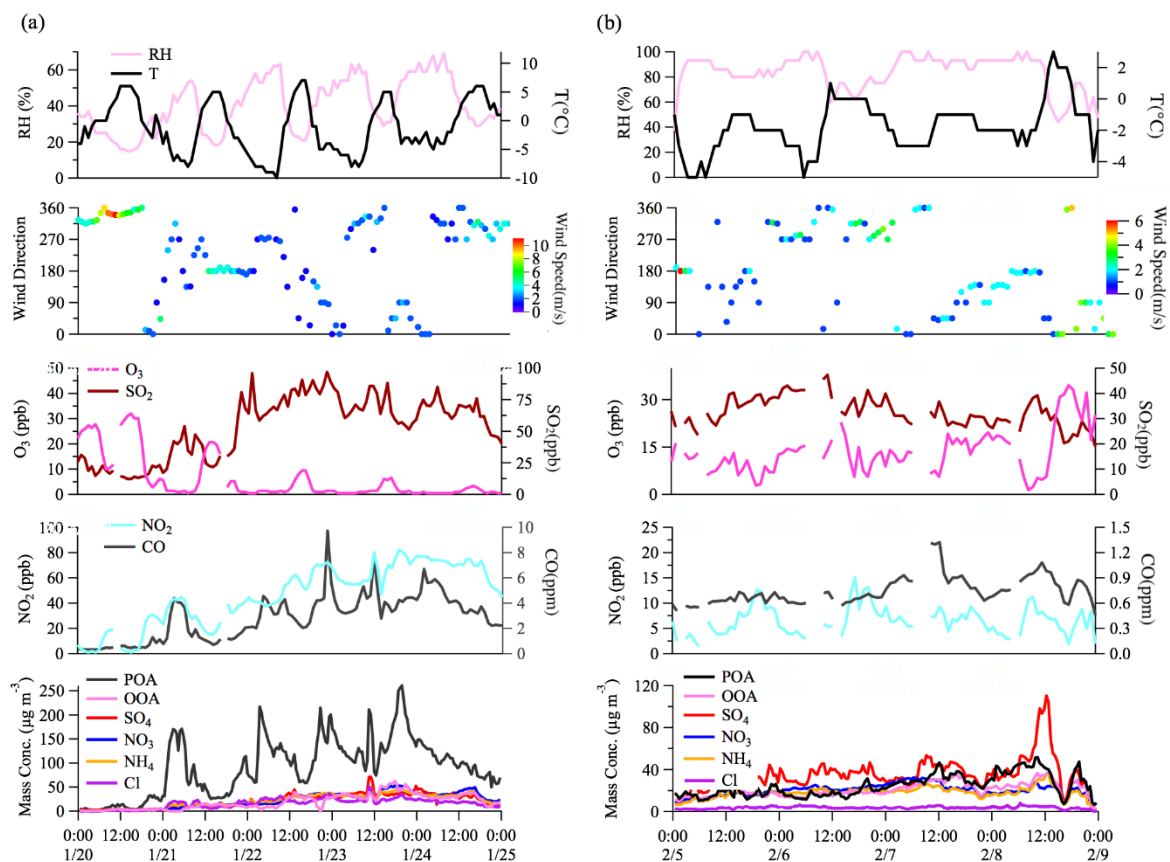
2 **Fig. 7. The average mass concentration of NR-PM₁ species (a) and OA sources (b) as a function**
 3 **of RH. The average mass concentration of NR-PM₁ species (c) and OA sources (d) normalized**
 4 **to the sum of primary sources (HOA, COA, BBOA, and CCOA) as a function of RH. All ratios**
 5 **are further normalized to the values at the first RH bin (<60%) for the better illustration.**

6



1

2 **Fig. 8. Summary of relative humidity and temperature, gaseous species, organic sources and**
 3 **NR-PM₁ chemical composition for high-RH (H1-H6) polluted, low-RH (L1-L4), and clean (C1-**
 4 **C4) episodes.**



1

2 **Fig. 9. Time series of meteorological factors (relative humidity, temperature, wind speed and**
 3 **wind direction), gaseous species, OA factors and NR-PM₁ chemical composition for the first**
 4 **period (average RH <50%) (a) and the second period (average RH >80%) (b).**